Multimuon production by muons

V. Barger and W. Y. Keung
Physics Department, University of Wisconsin, Madison, Wisconsin 53706

R. J. N. Phillips
Rutherford Laboratory, Chilton, Didcot, Oxon, England

(Received 22 January 1979)

We evaluate and compare the predictions of the principal mechanisms that are expected to produce multimuon signals $\mu N \to (n\mu)X$, namely (i) $\mu\bar{\mu}$ pair formation by bremsstrahlung and by photon-photon interaction, (ii) $c\bar{c}$ and $b\bar{b}$ heavy-quark production by photon-gluon fusion, and (iii) muon production by hadronic final-state interactions. We concentrate attention mainly on trimuons, but include some discussion of opposite-sign and same-sign dimuons, wrong-sign single muons, and diffractive ψ production.

I. INTRODUCTION

Multimuon production in μN scattering is interesting primarily as a means to study the associated production of charm and other heavy quarks. The initial $\mu N \to 2\mu X, 3\mu X$ events from Fermilab[1] have been discussed as a possible charm signal.[1,2] Higher-statistics experiments at Fermilab and CERN are currently being analyzed. It seems appropriate now to make a careful study of the mechanisms that can lead to multimuon events. In addition to the muon signals from charm decays, conventional processes contribute significant backgrounds through Bethe-Heitler,[3,4] bremsstrahlung,[4,5] and hadronic channels.[6,7] A systematic theoretical study of these background contributions is needed to isolate the charm-decay signals. In this paper, we quantitatively survey the background contributions and compare them with charm production in the photon-gluon-fusion model.[8]

II. ELECTROMAGNETIC AND HADRONIC BACKGROUNDS

To order α^4, muon pairs can be created electromagnetically by bremsstrahlung from the interacting particles and by the Bethe-Heitler (photon-photon-fusion) process. The Feynman diagrams are shown in Fig. 1; the sets of diagrams 1(a), 1(b), 1(c) are separately gauge invariant. The correction due to identical-fermion antisymmetrization in low-energy 17-GeV muon tridents on lead was calculated[3] to be 6% of the total cross section. We believe at higher energy this effect should be even smaller and we neglect it. Heavy-lepton pairs can be produced similarly, but the $\tau\bar{\tau}$ cross section is strongly suppressed relative to $\mu\bar{\mu}$, and hence the muonic decay modes of τ cannot contribute significantly to multimuon final states. Because of charge-conjugation invariance, there is no interference between Bethe-Heitler and bremsstrahlung diagrams in the total cross section; however, interference is present in differential cross sections and in acceptance-corrected integrated cross sections.

Previous calculations of the diagrams in Fig. 1 were based on the incoherent quark-parton model for the nucleon vertex, which would be appropriate for large momentum transfer Q_H to the hadron vertex. However, because of the virtual photon propagators, the dominant contributions to the cross section are at very low $Q_H^2 \ll 1$ GeV^2, so that the question of coherence becomes important. Therefore in addition to the parton-model calculations for a nucleon target, we also evaluate coherent scattering from a parton target and from an Fe target in which the target recoils without breakup.

In the parton model, the recombination of quarks into hadrons in the final state provides an addition-

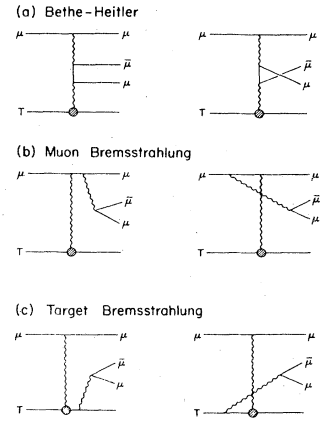

FIG. 1. Feynman diagrams for the electromagnetic process $\mu \to 3\mu$ for a target T; (a) Bethe-Heitler, (b) muon bremsstrahlung, (c) target bremsstrahlung.

 © 1979 The American Physical Society

al source of muon pairs, as illustrated in Fig. 2(a). This source is difficult to estimate from first principles, but can be largely related to muon pair production in πN scattering or to muon pairs from the hadronic vertex in neutrino deep-inelastic scattering.[6,7]

A. Parton target

Parton kinematics is introduced exactly as in the calculation of electromagnetic pair contributions to neutrino trimuon production, described in Ref. 9. The squared matrix elements for the diagrams of Fig. 1 are evaluated by standard computer trace techniques and the cross sections are integrated by Monte Carlo methods over all phase space with final hadronic invariant mass $W > m_N + m_\pi$.

The matrix elements vary rapidly with the squared momenta of the virtual photons, and hence experimental acceptance cuts are of critical importance. For all of our illustrations we take the typical acceptance cuts

$$E_\mu > 5 \text{ GeV} \quad \text{(all muons)}, \qquad \theta_\mu > 5 \text{ mrad} \quad \text{(leading muon)}. \tag{1}$$

An angular cut for the leading muon, defined as the fastest muon with the same sign as the beam, helps to avoid confusion with unscattered beam particles; with a magnetic field, an angular cut on the slower secondary muons is not usually necessary.

With the cuts of Eq. (1) the calculated single muon inclusive cross section at 280 GeV for an isospin-average nucleon target is

$$\sigma(\mu^- N \to \mu^- X) = 180 \text{ nb}. \tag{2}$$

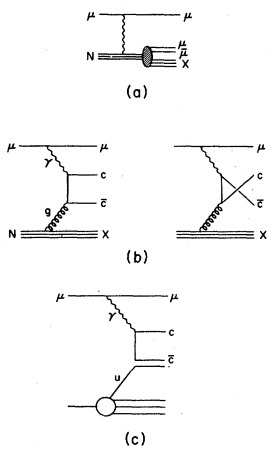

FIG. 2. Diagrams for (a) hadronic final-state interaction $\mu N \to 3\mu X$, (b) $c\bar{c}$ production by photon-gluon fusion, (c) nonperturbative charm production.

Over the incident energy range 150–300 GeV, the $\mu N \to 3\mu X$ cross sections increase slowly. It is interesting to compare the separate contributions of Bethe-Heitler and two kinds of bremsstrahlung graphs with the total cross section including all interferences. The values at 280 GeV without cuts and with acceptance cuts are as follows, for an isospin-average nucleon target:

3μ cross sections		no cuts	with cuts
σ(Bethe-Heitler)	=	1.1 nb	0.8×10^{-2} nb
$\sigma(\mu$ brems)	=	0.03 nb	0.5×10^{-2} nb
σ(quark brems)	=	0.03 nb	0.04×10^{-2} nb
σ(total 3μ)	=	1.2 nb	1.4×10^{-2} nb.

(3)

Comparing the sum of the first three entries with σ(total 3μ), we see that interference between these components is relatively small.

The acceptance cuts reduce the cross sections by orders of magnitude. The effect is most severe for the Bethe-Heitler and quark bremsstrahlung, where the leading μ tends to come out at small angles and the secondary muons are slow. The effect is least severe for muon bremsstrahlung, where the leading μ is distributed at larger angles and the secondary muons are fast. The $\sigma(\mu$ brems) becomes competitive with σ(Bethe-Heitler) after acceptance corrections, even though it was two orders of magnitude smaller before cuts.

The $\mu N \to \mu\tau\bar{\tau}X$ cross section at 280 GeV is

$$\sigma(\mu\tau\bar{\tau}) = 0.6 \times 10^{-3} \text{ nb, no cuts} \qquad = 0.2 \times 10^{-3} \text{ nb, with cuts on leading muon}, \tag{4}$$

which is negligible in comparison with 3μ rates.

The two dominant contributions $\sigma(\mu$ brem) and σ(Bethe-Heitler) have quite different dependences on $Q_\mu{}^2$, the squared momentum transfer to the leading muon. Figure 3 shows $d\sigma/dQ_\mu{}^2$ without acceptance cuts. At large $Q_\mu{}^2$, σ(Bethe-Heitler) becomes negligible. The corresponding dependences on $Q_H{}^2$ are also shown in Fig. 3. The fact that 90% of the calculated contribution comes from the region $Q_H{}^2 < 0.3$ (GeV)^2 means that the parton-model approach is questionable.

When the acceptance cuts hide one of the muons, the electromagnetic $\mu N \to 3\mu X$ cross section is observed as an apparent $\mu N \to 2\mu X$ signal. For opposite-sign dimuons, the Bethe-Heitler contribution dominates by a factor of 20. The result at 280 GeV for an isospin-average target is

$$\sigma(\mu^-\mu^+) \equiv \sigma(\mu^- N \to \mu^-\mu^+ X) = 0.7 \text{ nb}. \tag{5}$$

Same-sign dimuons are observed when one of the

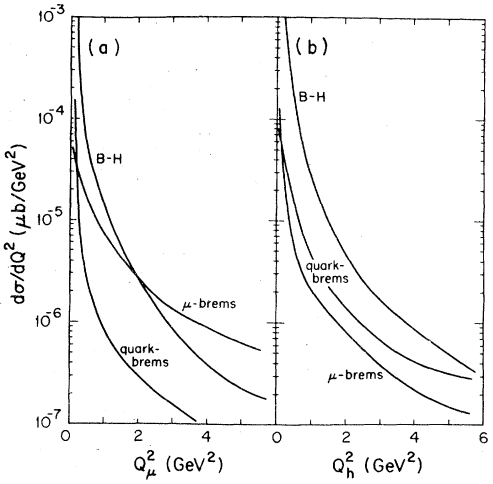

FIG. 3. Bethe-Heitler and μ brems parton-model cross sections (a) $d\sigma/dQ_\mu{}^2$ versus $Q_\mu{}^2$ the squared momentum transfer to the leading muon, (b) $d\sigma/dQ_H{}^2$ versus $Q_H{}^2$ the squared momentum transfer to the target. All curves are for $E=280$ GeV without acceptance cuts.

secondary muons from the pair is lost. Comparable contributions arise from Bethe-Heitler and bremsstrahlung graphs, but the net signal is extremely small:

$$\sigma(\mu^-\mu^-)\equiv\sigma(\mu^-N\to\mu^-\mu^-X)=1\times10^{-3}\text{ nb}. \tag{6}$$

When the acceptance cuts hide two muons of the same sign, the electromagnetic $\mu N\to3\mu X$ process is observed as an apparent wrong-sign single muon signal. The result at 280 GeV for an isospin-average nucleon is

$$\sigma(\mu^+)\equiv\sigma(\mu^-N\to\mu^+X)=0.2\text{ nb}, \tag{7}$$

based on the acceptance cuts of Eq. (1).

B. Hadronic final-state interactions

After an initial hard scatter from the incident muon, the struck quark undergoes multiple soft hadronic final-state interactions that cannot be calculated from first principles. However, the recombination of quarks into hadrons in the central region, via short-range rapidity interactions, is expected to be largely independent of the incident particles. Hence any muon pairs arising centrally in the final-state interaction (from meson decays or continuum conversions $q\bar{q}\to\gamma\to\mu\bar{\mu}$ or charm production $q\bar{q}\to c\bar{c}$) should occur with approximately the same relative probability as in πN scattering.

The above argument suggests that the hadronic component of trimuon production can be written in a factorized form[7]

$$\frac{d\sigma(\mu N\to\mu(\mu\bar{\mu})X)}{dx\,dy\,d^3p\,dm}=\frac{d\sigma(\mu N\to\mu X')}{dx\,dy}\frac{\lambda}{\sigma_{\text{tot}}(\pi N)}\frac{d\sigma(\pi N\to(\mu\bar{\mu})X)}{d^3p\,dm}, \tag{8}$$

where the πN cross section is at the same total energy and vector momentum as the hadronic final state X' of interest, with the longitudinal axis aligned along the axis of momentum transfer. Here x,y are the usual Bjorken scaling variables; p and m are the momentum and mass of the muon pair. The parameter λ is expected to be of order 1.

In Ref. 7 a parametrization of $\pi N\to\mu\bar{\mu}X$ was presented and applied to the analogous problem of neutrino-trimuon production; an empirical value $\lambda=2.5$ was found to represent the relevant neutrino data adequately, with the assumption that all $\mu\bar{\mu}$ pairs decay isotropically. In the present paper we adopt the same πN parametrization and assumptions as in Ref. 7, with the same value $\lambda=2.5$.

Since the virtual photons in multimuon production turn out to have small Q^2, an alternative justification of the above model is ρ-meson dominance of the photon coupling plus the similarity of ρN and πN interactions in the central region.

Some of the central hadronic dimuons presumably come from associated charm production with semileptonic decays, but such contributions are quite distinct from those of photon-gluon fusion discussed later. The electromagnetic current is absorbed in one case by a light quark, in the other case by a charmed quark. There is no double counting.

The hadronic final-state interaction cross sections at 280 GeV, with the acceptance cuts of Eq. (1), are

$$\begin{aligned}&\sigma(\text{hadronic }3\mu)=0.9\times10^{-2}\text{ nb},\\&\sigma(\text{hadronic }\mu^+\mu^-)=4.0\text{ nb},\\&\sigma(\text{hadronic }\mu^-\mu^-)=0.5\times10^{-2}\text{ nb},\\&\sigma(\text{hadronic }\mu^+)=14.5\text{ nb}.\end{aligned} \tag{9}$$

The dimuon cross sections here are for misidentified trimuons only. Presumably there are also some true dimuons from hadronic charm production, with one muonic and one nonmuonic charm decay, but we do not have enough information to calculate them.

C. Diffractive mechanism

Our final-state-interaction model fails to include some leading-particle effects in the hadronic vertex, notably the quasielastic production of neutral vector mesons

$$\gamma N \to V^0 N \quad (V = \rho, \omega, \phi, \psi \cdots),$$

with leptonic decays $V \to \mu^+\mu^-$. In a simple vector-dominance approach, neglecting longitudinal terms, the diffractive cross section is

$$\frac{d\sigma(\mu N \to \mu V N)}{dx\,dy\,dt} = \frac{3 m_N m_V^3 E\,\Gamma(V \to e^+e^-)}{8\pi^2 Q^2 (Q^2 + m_V^2)^2} [\sigma_{\text{tot}}(VN)]^2 \times \exp(B_V t)(1 - y + \tfrac{1}{2} y^2) \times \theta(W - m_N - m_V). \tag{10}$$

Here t is the invariant momentum transfer squared in the virtual $\gamma N \to VN$ scattering and W is the invariant hadronic mass $W^2 = 2MEy(1-x) + m_N^2$. The slope parameters B_V in Eq. (10) are given in terms of the total cross sections by the empirical formula[10]

$$B_V^2 \simeq 2.5\,\sigma_{\text{tot}}(VN), \tag{11}$$

where B_V is in GeV^{-2} and σ_{tot} is in mb. A comparable contribution may be expected from diffraction dissociation at the nucleon vertex $\gamma N \to VN^*$.

Since these processes have unique experimental signatures (essentially all the incident energy emerges on the three muons, and one $\mu^+\mu^-$ pair has invariant mass m_V), we do not pursue their calculation further, concentrating instead on the more elusive continuum pair contributions. The case of ψ production has particular interest in its relation to charm production mechanisms. We return to it later in the photon-gluon model.

D. Coherent proton target

The preceding parton-target calculations point to the dominance of small Q_H^2 and hence to the likelihood of a coherent recoil of a struck proton. Our parton-model calculations with $W > m_N + m$ were intended to represent breakup of the struck nucleon; hence coherent recoil of the nucleon as a whole is additive.

For coherent proton recoil, we use the dipole electromagnetic form factors; the coherent neutron contribution is negligible. The calculated elastic proton scattering cross section at 280 GeV for the acceptance cuts of Eq. (1) is

$$\sigma(\mu^- p \to \mu^- p) = 100 \text{ nb} \tag{12}$$

The trimuon cross sections at 280 GeV are

3μ cross sections		no cuts	with cuts
σ(Bethe-Heitler)	=	6.0 nb	1.3×10^{-2} nb
$\sigma(\mu$ brems)	=	0.7×10^{-1} nb	0.5×10^{-2} nb
$\sigma(N$ brems)	=	0.1×10^{-1} nb	0.6×10^{-6} nb.

(13)

The bremsstrahlung from the nucleon target is sufficiently small to ignore. The apparent dimuon and wrong-sign single-muon cross sections are strongly dominated by the Bethe-Heitler process: The results at 280 GeV are

$$\sigma(\mu^-\mu^+) = 2.2 \text{ nb},$$
$$\sigma(\mu^-\mu^-) = 0.3 \times 10^{-2} \text{ nb}, \tag{14}$$
$$\sigma(\mu^+) = 0.9 \text{ nb}.$$

The net 3μ and 2μ cross sections in Eqs. (13) and (14) for a coherent proton target are comparable to the incoherent parton-model results of Eqs. (3)–(7). Since the latter were restricted to $W > m_N + m$, there is no double counting in principle.

E. Coherent Fe target

Some of the muon scattering measurements are being made with Fe targets. For these experiments we must examine the importance of coherent scattering from the complex nucleus. We can only simply treat the case of elastic nuclear recoil (no breakup or excitation), using the electromagnetic nuclear form factor of Ref. 1. The resulting 3μ cross sections *per nucleon* at 280 GeV are

3μ cross sections		no cuts	with cuts
σ(Bethe-Heitler)	=	11 nb	0.12×10^{-1} nb
$\sigma(\mu$ brems)	=	0.3 nb	0.07×10^{-1} nb.

(15)

The apparent dimuon and wrong-sign single-muon cross sections from this source originate dominantly from the Bethe-Heitler term and are

$$\sigma(\mu^-\mu^+) = 8 \text{ nb/nucleon},$$
$$\sigma(\mu^-\mu^-) = 1 \times 10^{-4} \text{ nb/nucleon}, \tag{16}$$
$$\sigma(\mu^+) = 1 \text{ nb/nucleon}.$$

The coherent Fe cross sections dominate over the proton and parton results. As an approximation, one might take the view that the proton target cross section weighted by $Z/A = 26/56$ represents the incoherent scattering on Fe per nucleon, and that the isospin-averaged parton cross section of

Eq. (2) represents the incoherent scattering with particle production.

III. HEAVY-QUARK PRODUCTION BY PHOTON-GLUON FUSION

In the framework of quantum chromodynamics (QCD), heavy-quark production estimates have been made on the basis of photon-gluon fusion,[8] shown in Fig. 2(b). The heavy quarks can decay semileptonically to produce multimuon events.

In our calculations, we assume a scaling on-shell gluon distribution

$$G(x)=3x^{-1}(1-x)^5\,, \tag{17}$$

where x is the nucleon momentum fraction carried by the gluon in an infinite-momentum frame. We take a constant gluon–heavy-quark coupling constant with scale set by the heavy-quark mass,

$$\alpha_s=\frac{12\pi}{(33-2n)\ln(4m_Q{}^2/\Lambda^2)}\,, \tag{18}$$

where n is the effective number of flavors and $\Lambda\simeq 0.5$ GeV. For the charmed quark c we take $m_c=1.87$ GeV $=m_D$ in order to get the correct $D\bar{D}$ threshold; with $n=4$ we then have $\alpha_s=0.37$. For the b quark we take $m_b=5$ GeV, $n=5$ and $\alpha_s=0.27$. Figure 4 shows the resulting $c\bar{c}$ and $b\bar{b}$ production cross sections from the photon-gluon mechanism versus incident energy E. This is a typical theoretical ansatz[8]; since the cross section is strongly weighted toward low Q^2, scale-breaking effects are minimized. Changing the power of $(1-x)$ in the gluon distribution to $(1-x)^3$ or $(1-x)^7$ causes only 10% deviations in the results for the total cross section and the $c\bar{c}$ distributions. The nonscaling "counting rule" distribution used by Gluck and Reya[8] leads to a factor of 20% reduction in the cross section due principally to the lower gluon normalization; however, the shapes of the distributions and the energy dependence of the cross section are closely similar to our present results.

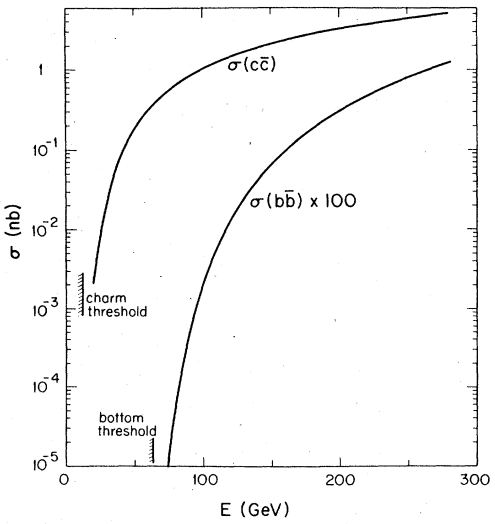

FIG. 4. Cross sections for $\mu N\to c\bar{c}X$ and $\mu N\to b\bar{b}X$ versus incident energy calculated in the photon-gluon fusion model. The $b\bar{b}$ result is scaled up by a factor of 100.

The multimuon cross sections arising from $c,\bar{c}$ decays are

$$\frac{\sigma(3\mu)}{B_\mu{}^2}=\frac{\sigma(\mu^+\mu^-)}{B_\mu(1-B_\mu)}=\frac{\sigma(\mu^-\mu^-)}{B_\mu(1-B_\mu)}=\sigma(c\bar{c})\,, \tag{19}$$

where B_μ is the $c\to\mu X$ branching fraction. In the case of $b\bar{b}$ production, the possibility of $b\to c\to s$ cascade decays leads to 2μ, 3μ, 4μ, and 5μ signals, but the production cross section in Fig. 4 suggests that these signals will be very small.

To predict the energy and angle distributions of the decay muons, a more detailed analysis is needed. We assume a c-quark-to-D-meson fragmentation function[11] $\mathfrak{D}(z)=$ constant, where $z=E_D/E_c$ in the laboratory frame; $\mathfrak{D}(z)$ is normalized to give one D meson per c quark. For the semileptonic decay of the D meson, we take equal proportions of $D\to K^*(0.89)\mu\nu$ and $D\to K\mu\nu$ with matrix elements from Ref. 12. For the semileptonic branching fraction $B(D\to\mu X)$ we take 10%.

The calculated μ^-N cross sections at $E=280$ GeV are $\sigma(\bar{c}c)=5$ nb and

		no cuts	with cuts
$\sigma(3\mu)$	=	0.5×10^{-1} nb	0.03×10^{-1} nb
$\sigma(\mu^-\mu^+)$	=	0.5 nb	0.6×10^{-1} nb
$\sigma(\mu^-\mu^-)$	=	0.5 nb	0.6×10^{-1} nb
$\sigma(\mu^+)$	=	0	1.1×10^{-1} nb.

(20)

In addition to photon-gluon fusion of order α_s, other low-order QCD diagrams can contribute to associated charm production. Gluon bremsstrahlung of $c\bar{c}$ pairs is of order $\alpha_s{}^2$ and proves to be negligible. It has been argued that nonperturbative QCD diagrams such as that of Fig. 2(c) may contribute very significantly.[13] There are considerable uncertainties in the evaluation of these diagrams and their overall strength is not known; however, their gross kinematical structure is similar to photon-gluon fusion (except that c comes always from the γ vertex, and the c and $\bar{c}$ are no longer symmetrical). The photon-gluon-fusion model is therefore the minimal expected charm contribution, and may need to be scaled up. The muon

experiments in progress could help to settle this important issue regarding nonperturbative QCD contributions.

IV. COMPARISONS

In the foregoing paragraphs we have surveyed the multimuon cross sections that might be expected from electromagnetic and charm sources. In this section we compare and contrast the various components and discuss how to discriminate among them.

We shall illustrate cross sections *per nucleon* [with and without cuts of Eq. (1)] for the following sources:

(i) *Electromagnetic quark* (q). The sum of Bethe-Heitler plus all bremsstrahlung terms in the quark-parton model for an isospin-average nucleon.

(ii) *Electromagnetic proton* (p). Bethe-Heitler plus μ brems for a coherent proton target.

(iii) *Electromagnetic*; *iron* (Fe). Bethe-Heitler plus μ brems for a coherent Fe target.

(iv) *Hadronic final-state interaction* (H). As in Sec. II B. We illustrate this only with acceptance cuts, since it is nearly singular otherwise.

(v) *Charm* ($c\bar{c}$). As in Sec. III.

For scattering from a hydrogen target the sum of (i), (ii), (iv), and (v) is appropriate. For an Fe target a possible approximation is to weight (ii) by $Z/A = 26/56$ and add (iii).

A. Trimuons

The foregoing results have shown that, with or without cuts, the integrated charm contribution

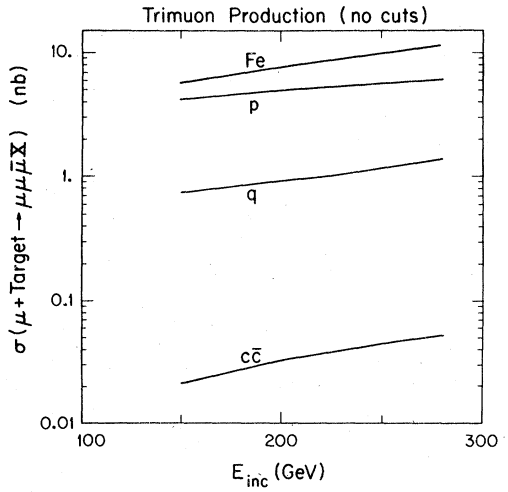

FIG. 5. Component trimuon cross sections per nucleon versus E without cuts; the curves are labeled according to the notation in Sec. IV.

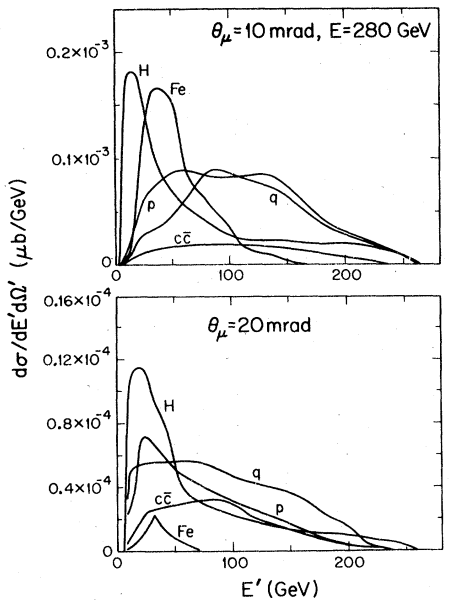

FIG. 6. Differential trimuon cross sections $d\sigma/d\Omega' dE'$ for the leading muon versus E' at fixed angles $\theta' = 10, 20$ mr; energy cuts $E_\mu > 5$ GeV have been used.

lies one or two orders of magnitude below the electromagnetic and hadronic backgrounds in the $E = 200$–300 GeV region. We therefore examine some differential distributions.

Figure 5 shows $\mu^- N \to 3\mu N$ cross sections per

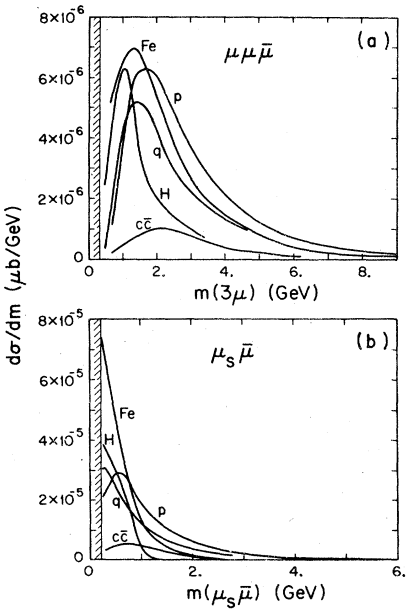

FIG. 7. Trimuon invariant-mass distributions at $E = 280$ GeV, with cuts (a) $d\sigma/dm(3\mu)$ versus $m(3\mu)$, (b) $d\sigma/dm(\mu^+\mu_S^-)$ versus $m(\mu^+\mu_S^-)$.

nucleon versus incident energy E, without cuts. Figure 6 shows the 280-GeV differential cross sections $d\sigma/d\Omega' dE'$ versus E' at fixed angles $\theta' = 10, 20$ mr, where Ω', E', θ' refer to the leading μ^-; energy cuts $E_\mu > 5$ GeV have been imposed. Figure 7 illustrates distributions with cuts imposed for the invariant masses $m(3\mu)$, $m(\mu^+\mu_S^-)$, where μ_S^- denotes the slow nonleading μ^-. Note that the latter discriminates between charm and hadronic components.

Figure 8 gives the distributions in the total energy E carried by the three final-state muons for the quark, hadronic, and charm sources. The p and Fe sources are sharply peaked at the incident energy $E = 280$ GeV. With cuts the mean $E(3\mu)$ energies from the different sources are

Source	$\langle E(3\mu)\rangle$
q	268 ± 27 GeV
p	280.0 ± 0.2 GeV
Fe	280.00 ± 0.02 GeV
H	134 ± 65 GeV
$c\bar{c}$	128 ± 51 GeV.

Thus 3μ events from coherent proton and Fe scattering should be easily identifiable from the characteristic $E(3\mu) \simeq E$. Since the bulk of the energy is carried by the muons in the electromagnetic cases, cutting on the summed energy $E(3\mu)$ offers a clean way to eliminate these backgrounds.[1]

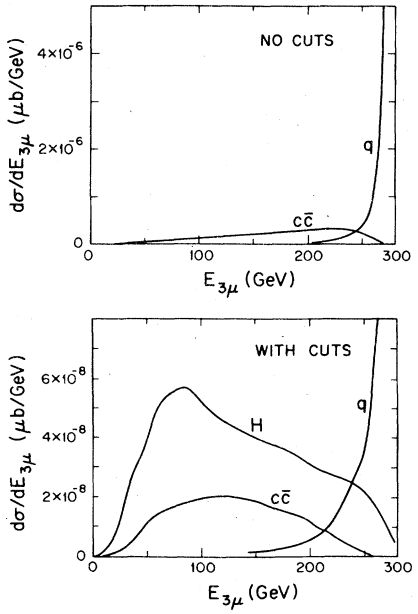

FIG. 8. Distributions in the total energy $E_{3\mu}$ carried by the final-state trimuons for the quark, hadronic, and charm sources.

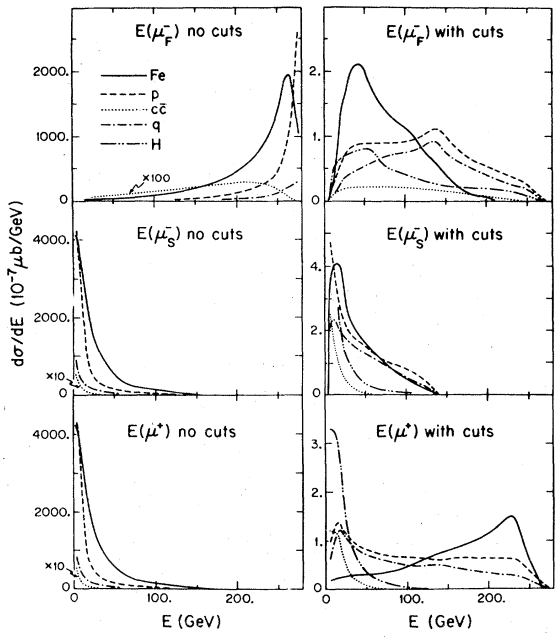

FIG. 9. Dependence on the energy of the fast $\mu^-(\mu_F^-)$, the slow $\mu^-(\mu_S^-)$, and the μ^+ in trimuon production at $E = 280$ GeV.

Figure 9 shows individual muon energy distributions at $E = 280$ GeV. The uncut electromagnetic distributions show the expected peaking of the direct μ^- near maximum, with the μ^+ peaking near zero; the slow μ^- is similar to μ^+. The acceptance cuts of Eq. (1)—especially the angle cut—have dramatic effects, essentially destroying the high-energy direct μ^- peak and distorting the μ^+ and slow μ^- curves accordingly.

Figure 10 shows the azimuthal correlations about the beam axis between the leading muon and the center of mass of the secondary muon pair; the Fe source which is not shown peaks sharply at $\phi = \pi$.

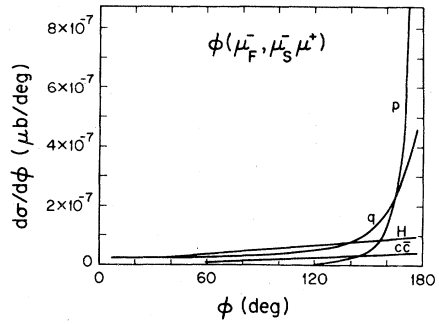

FIG. 10. Azimuthal correlations for trimuons between the leading muon and the muon momentum of the secondary muon pair for $E = 280$ GeV with cuts.

B. Dimuons

Opposite-sign dimuon production $\mu^- N \to \mu^- \mu^+ X$ is again heavily dominated by electromagnetic and hadronic backgrounds. Figure 11 shows the predicted energy and invariant mass distributions at $E = 280$ GeV. Figure 12 shows the azimuthal correlation about the beam axis. The charm signal can be enhanced by additional cuts on energy, azimuth, and invariant mass, but clean identification seems difficult.

Same-sign dimuons are another story, however. For the electromagnetic and hadronic mechanisms, when both μ^- have passed the acceptance of Eq. (1), the remaining μ^+ is biased fast and is almost certain to be detected. Hence $\mu^-\mu^-$ is suppressed for the background mechanisms and charm production surprisingly dominates. Figure 12 also shows the predicted azimuthal correlations for $\mu^-\mu^-$ events. Figure 13 gives energy distributions for same-sign dimuons; for proton and Fe targets, the $E(\mu^-\mu^-)$ distribution peaks sharply at the incident energy.

Essentially charm dominates $\mu^-\mu^-$ because it can give *true* dimuons, whereas the background mechanisms contribute only via misidentified trimuons. Strictly speaking, charm production in hadronic final-state interactions can also contribute true dimuons as noted earlier; we have omitted this component simply for lack of information.

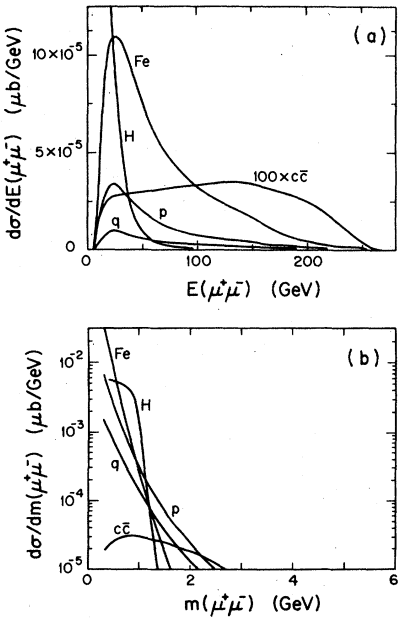

FIG. 11. Opposite-sign dimuon distributions at $E = 280$ GeV with cuts (a) $d\sigma/dE(\mu^+\mu^-)$, (b) $d\sigma/dm(\mu^+\mu^-)$.

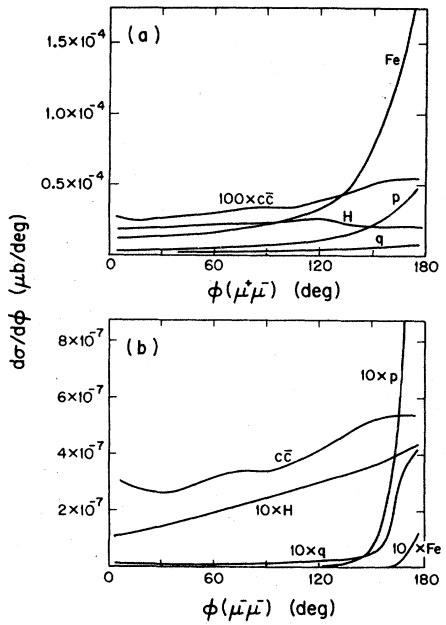

FIG. 12. Azimuthal correlations for dimuons at $E = 280$ GeV with cuts (a) $d\sigma/d\phi(\mu^+\mu^-)$, (b) $d\sigma/d\phi(\mu^-\mu^-)$.

C. Wrong-sign muons

Wrong-sign single-muon production $\mu^- N \to \mu^+ X$ is dominated by the electromagnetic background, given the acceptance cuts of Eq. (1). For $E = 280$ GeV, the dependence on the final muon energy

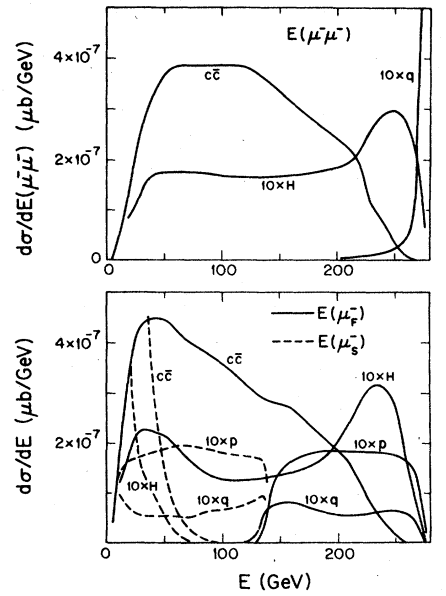

FIG. 13. Distributions for $E(\mu^-\mu^-)$, $E(\mu_F^-)$, and $E(\mu_S^-)$ in $\mu^- N \to \mu^-\mu^- X$ events.

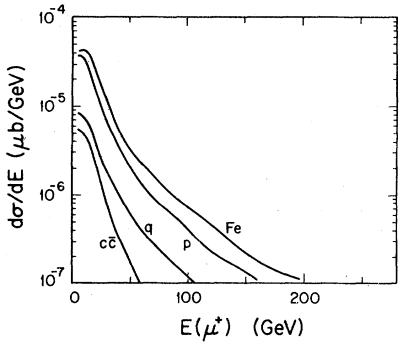

FIG. 14. Energy distributions of wrong-sign single muon $d\sigma/dE(\mu^+)$ at $E=280$ GeV.

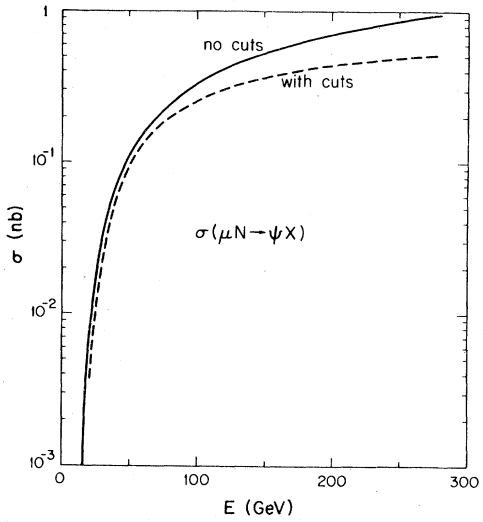

FIG. 15. Estimated ψ-production cross section versus energy with and without acceptance cuts on the direct muon only.

$E(\mu^+)$ is shown in Fig. 14; the hadronic source which is not shown peaks extremely sharply at $E(\mu^+)=5$ GeV.

V. ψ PRODUCTION

It has been argued[8] that all $c\bar{c}$ production is approximately described by photon-gluon fusion, and that bound $c\bar{c}$ states can be included by lowering the charm threshold from $2m_D$ to $2m_c$ (a soft gluon can be radiated to achieve C-odd final states.) Since there are about 8 bound $c\bar{c}$ states, we guess that $\frac{1}{8}$ of the cross section goes directly to ψ production, while evidence from $pp\to\psi X$ data[14] suggests that an equal number of ψ states arise from the decay of P-wave χ states. There is also some contribution from $\psi'\to\psi$ cascades. Figure 15 shows the estimated ψ-production cross section based on this approach (taking $\frac{1}{4}$ of bound $c\bar{c}$ production), with and without acceptance cuts on the direct muon only. These values must be multiplied by the branching fraction $B(\psi\to\mu\mu)=0.07$ to give trimuon cross sections. ψ' production may be estimated similarly: Here there is no P-state contribution and the muon branching fraction is $B(\psi'\to\mu\mu)=0.008$. The trimuon rate of ψ' origin should be suppressed by a factor of order 20.

The photon-gluon mechanism above essentially represents diffractive ψ production; it is arguably more reliable than vector-dominance calculations, since the latter would require large mass extrapolations. In addition, we may expect some central hadronic ψ production; this gives a very small component of hadronic dileptons and was omitted from the model of Ref. 7 used in Sec. II B.

VI. CONCLUSIONS

Our conclusions may be summarized as follows:

(i) Bethe-Heitler and bremsstrahlung mechanisms give big trimuon-production cross sections for typical acceptance cuts.

(ii) Target coherence is very important for these electromagnetic processes and enhances their cross sections considerably.

(iii) Lepton pair production by hadronic final-state interactions is another strong source of trimuons.

(iv) Acceptance cuts are very important and can produce dramatic effects. Because of cuts, $\mu^-\mu^-\mu^+$ trimuon events can be misidentified as $\mu^-\mu^+$, $\mu^-\mu^-$, or μ^+ events.

(v) The charm-trimuon signal expected from photon-gluon fusion is much smaller than the electromagnetic and hadronic backgrounds. The electromagnetic background can be eliminated by excluding the highest values of $E(3\mu)$, and the hadronic background by cutting on $m(\mu^+\mu_S^-)$.

(vi) The charm-dimuon signals are enhanced relative to 3μ, because of the greater probability of nonmuonic charm decays. Noncharm background dimuon signals are suppressed relative to the 3μ, because they are essentially misidentified 3μ events. With the acceptance cuts of Eq. (1) the charm $\mu^-\mu^+$ signal is small compared to background, and difficult to separate experimentally. The charm $\mu^-\mu^-$ signal dominates over noncharm background.

(vii) Wrong-sign single muons $\mu^-N\to\mu^+X$ are dominated by noncharm backgrounds.

(viii) There is an additional source of true dimuons coming from hadronic final-state charm production with only one muonic charm decay that we have not calculated for lack of information. These are distinct from charm dimuons of photon-

gluon origin but probably difficult to separate experimentally. This source also contributes apparent wrong-sign single muons that we have not calculated.

(ix) The photon-gluon-fusion mechanism provides an estimate of diffractive ψ production, shown in Fig. 15.

(x) Multimuons from $\tau\bar{\tau}$ and $b\bar{b}$ production are negligible.

ACKNOWLEDGMENTS

We thank T. Gottschalk for assistance during the initial phase of this work. This research was supported in part by the University of Wisconsin Research Committee with funds granted by the Wisconsin Alumni Research Foundation, and in part by the Department of Energy under Contract No. EY-76-C-02-0881, COO-881-83.

[1]K. W. Chen, in *Proceedings of the International Conference on Production of Particles with New Quantum Numbers*, Madison, Wisconsin, 1976, edited by D. B. Cline and J. J. Kolonko (Univ. of Wisconsin, Madison, 1976); K. W. Chen and A. Van Ginneken, Phys. Rev. Lett. 40, 1417 (1978).

[2]V. Barger and R. J. N. Phillips, Phys. Lett. 65B, 167 (1976); F. Bletzacker *et al.*, Phys. Rev. Lett. 37, 1316 (1976); S. Nandi and H. R. Schneider, Phys. Rev. D 15, 3247 (1977); D. P. Roy, Phys. Lett. 68B, 76 (1977).

[3]M. Tannenbaum, Phys. Rev. 167, 1308 (1968); S. Brodsky and S. Ting, *ibid.* 145, 1018 (1966).

[4]K. J. Evans, Nucl. Phys. B75, 171 (1974).

[5]V. Ganapathi and J. Smith, Phys. Rev. D 19, 801 (1979).

[6]T. Hansl *et al.*, Nucl. Phys. B142, 381 (1978).

[7]V. Barger *et al.*, Phys. Rev. D 18, 2308 (1978).

[8]L. M. Jones and H. W. Wyld, Phys. Rev. D 17, 759, 2332 (1978); J. Babcock *et al.*, *ibid.* 18, 162 (1978); M. A. Shifman *et al.*, Nucl. Phys. B136, 157 (1978); H. Fritzsch and K. Streng, Phys. Lett. 72B, 385 (1978); M. Gluck and E. Reya, *ibid.* 79B, 453 (1978); J. Leveille and T. Weiler, Nucl. Phys. B147, 147 (1979).

[9]V. Barger *et al.*, Phys. Rev. D 17, 2284 (1978).

[10]V. Barger and R. J. N. Phillips, Nucl. Phys. B97, 452 (1975).

[11]R. Odorico and V. Roberto, Nucl. Phys. B136, 333 (1978).

[12]V. Barger *et al.*, Phys. Rev. D 16, 746 (1977).

[13]F. Halzen and D. M. Scott, Phys. Lett. 72B, 404 (1978).

[14]J. Cobb *et al.*, Phys. Lett. 72B, 497 (1978); L. Holloway *et al.*, reported to XIX International Conference on High Energy Physics, Tokyo, 1978 (unpublished).